Renewable Energy 74 (2015) 855–866

Contents lists available at ScienceDirect

Renewable Energy

journal homepage: www.elsevier.com/locate/renene

Optimization of Stirling engine design parameters using neural networks

M. Hooshang [a, b], R. Askari Moghadam [a, *], S. Alizadeh Nia [b], M. Tale Masouleh [a, c]

[a] Faculty of New Sciences and Technologies, University of Tehran, Tehran, Iran
[b] Stirling Engine Laboratory, Irankhodro Power Train Company, Tehran, Iran
[c] Human and Robot Interaction Laboratory, Faculty of New Sciences and Technologies, University of Tehran, Iran

ARTICLE INFO

Article history:
Received 14 August 2013
Accepted 7 September 2014
Available online

Keywords:
Stirling engine
Optimization
Neural networks

ABSTRACT

This paper presents a new optimization procedure for Stirling engines based on neural network concepts. Based on modeling and experimental data an intelligent and fast method is proposed which finds the best values for different design variables. Design variables of Stirling engine are optimized using Multi-Layer Perceptron (MLP) neural networks. The optimization procedure is performed for three typical design variables for a given precision which has the capability to be extended for various types of engines and designs.

Design variables are assumed to be *phase angle*, *displacer stroke* and *working frequency* of *ST500* Stirling engine. Output variables which are subject to be optimized are the engine *output power* and *efficiency*. Maximizing a weighted average of these output variables is defined as total procedure objective.

Usually, output variables are calculated using mathematical modeling based on structure, drive mechanism, dynamics and thermodynamic properties of the Stirling engine. The Multi-Layer Perceptron network is trained via 125 samples of design and output variables, generated by *Nlog thermodynamic analysis code*, in order to learn the relations between them. Then, the maximum point for the weighted average of the network outputs is determined with adequate precision. The proposed optimal point for the Stirling engine finally is substituted into the analysis code, and its outcome is compared with network results at this point. The proposed values are validated by analysis code. In order to check the validation of *Nlog* analysis code results for this scope of study, a test setup for *ST500* engine is also established. Absolute pressure of working fluid and crank angle of the engine are measured instantly for three different charge pressures and compared with analysis results.

© 2014 Elsevier Ltd. All rights reserved.

1. Introduction

Stirling engines have found a variety of applications as energy converters for Stirling/Dish, residential CHP, coolers and heat pumps etc. Specially, as renewable energy and energy efficiency have become more critical areas of research in recent years, the design and development of Stirling engine systems has been signified for combined heat and power systems.

The ideal Stirling cycle, as illustrated in Fig. 1, is an idealized thermodynamic cycle, involves four thermodynamic processes, including two isothermal and two constant volume processes [1].

The theoretical efficiency of a Stirling cycle operating between high temperature T_e and low temperature T_c is the same as that of a Carnot cycle. Heat is delivered to the cycle at T_e, part of the heat is converted to work and the rest is removed as rejected heat at T_c.

Carnot revealed in 1820s that the maximum efficiency available from an engine working under this cycle depends only on the temperature difference in the cycle according to Eq. (1) which is called Carnot cycle efficiency.

$$\eta = 1 - \frac{T_c}{T_e} \tag{1}$$

* Corresponding author.
E-mail addresses: mazdak_hooshang@live.com (M. Hooshang), r.askari@ut.ac.ir (R. Askari Moghadam), s.alizadehnia@ip-co.com (S. Alizadeh Nia), m.t.masouleh@ut.ac.ir (M.T. Masouleh).

http://dx.doi.org/10.1016/j.renene.2014.09.012
0960-1481/© 2014 Elsevier Ltd. All rights reserved.

Nomenclature

U	network input
Y	network output
ξ	network output-layer weight
w	network mid-layer weight
W	optimization weighting vector
Γ	engine performance
I	number of network mid-layer neurons
i	neuron index ($i = 1,2,\ldots,I$)
J	number of network inputs
j	network input index ($j = 1,2,\ldots,J$)
H	number of network outputs
h	network output index ($h = 1,2,\ldots,H$)
σ	sum of network input signals (m)
γ	network learning rate
δ	network deviation factor
q	total network training samples
z	number of grid points along each input axis
θ	Crank angle (Radian)
φ	piston-displacer phase angle (Radian)
l_1	piston rod length (m)
l_2	displacer rod length (m)
a_1	piston gudgeon pin & surface distance (m)
a_2	displacer gudgeon pin & surface distance (m)
a_3	displacer height (m)
b_1	piston gudgeon pin & crank axis distance (m)
b_2	displacer gudgeon pin & crank axis distance (m)
c_1	piston cylinder head & crank axis distance (m)
c_2	displacer cylinder head & crank axis distance (m)
d	displacer stroke (cm)
r_c	Crank radius (m)
A_f	gas flow area (m^2)
f	engine frequency (Hz)
η	engine efficiency
p	engine output power (W)
Q_r	total heat rate rejected from the engine (W)
T_c	heat rejection temperature ($^\circ$K)
T_e	heat absorption temperature ($^\circ$K)
v_f	gas velocity(m/s)
ρ	gas density(kg/m^3)
n	control-volume normal surface vector
x	control-volume length(m)
A_w	wall area of control-volume (m^2)
S	connecting surfaces between adjacent control-volumes (m^2)
V	volume of control-volume (m^3)
T	gas temperature inside control-volume ($^\circ$K)
P	gas pressure inside control-volume (Pa)
τ_f	gas shear stress from control-volume wall (Pa)
u	gas specific internal energy (J/kg)
Q_c	net absorbed heat of control-volume gas (J)
Q_e	net injected heat to control-volume (J)
m_w	mass of control-volume wall (kg)
c_w	specific heat of control-volume wall (kJ/kg)
T_w	temperature of control-volume wall ($^\circ$K)
r	working gas constant (kJ/kg.K)
c_v	gas specific heat for constant volume (kJ/kg.K)
Re	Reynolds number of control-volume gas
Re_w	Reynolds number of control-volume gas
μ	viscosity of control-volume gas (Pa.s)
Nu	Nusselt number
k	control volume index
K	working gas conductivity (w/m.K)
t	time (s)

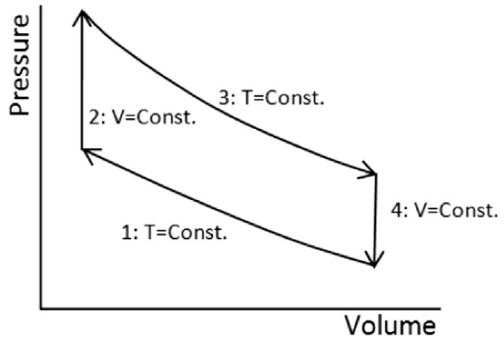

Fig. 1. Ideal Stirling engine cycle processes.

The efficiency of a real Stirling engine is also determined through measuring power output and rejected heat according to Eq. (2) as follows: [1]

$$\eta = \frac{p}{\dot{Q}_r + p} \tag{2}$$

More than twenty sets of parameters like pressure, temperatures, engine working frequency, power piston and displacer geometries, heat-exchanger geometries have direct effect on engine output power and efficiency and they complicate the design procedure.

In other words, one of the important issues about designing a Stirling engine is to find an algorithm to find proper values of the engine parameters in order to optimize the engine performance [2].

In order to find the best design point, the simplest method consists in assuming all possible situations for engine specifications and checking the engine performance at each point. The main problem in this approach is the large number of unknown specifications. Thus calculating the effect of each parameter by means of convenient methods, needs a significant time which makes this method irrational.

In principle, designing an engine starts with finding a set of parameters based on experiences and the next step is optimization for other parameters to improve the performance [3].

Toropov has utilized the simplified approximations of the original objective/constraint functions, obtained by the weighted least-squares method [4]. It used the information about function values gained at several previous design points in order to improve the quality of simplified approximations to the end of reducing the total number of calls for complex engineering systems analyses.

Hirata has studied the effect of some heat losses and irreversibility on the engine performance indices [5]. He has calculated the optimal performance and design parameters for maximum power and efficiency. It was considered that a compact Stirling engine was optimized by detailed measurements for heat balance.

Timoumi et al. have carried out an optimization of GPU-3 engine data [6]. It resulted in reduction of the losses and to a notable improvement in the engine performance. The parameters of this

prototype were first applied on the developed model; the results were very close to the experimental data. Then, the influence of each geometrical and physical parameter on the engine performance and the exchanged energy of the regenerator were studied.

Mahkamov et al. have developed a mathematical model of the LTD[1] Stirling engine which accounts for hydraulic and heat losses in the working process and mechanical losses in the engine [7]. This model was optimized by Genetic Algorithm. As a result, a set of design parameters for the engine was obtained which provides a considerable improvement in the performance. Results were calibrated using 3D CFD modeling technique.

Chen et al. have introduced finite-time thermodynamics to optimize the performance of a solar powered Stirling engine [8]. The genetic algorithm is used to reveal the maximum output power of a Stirling engine by determining the thermal efficiency, the collector temperature and their corresponding values of the optimized parameters. The results of the simulation herein described can be directly applied to optimize the design of a practical solar powered Stirling engine.

All of the discussed optimization algorithms are classified in gradient or evolutionary category. The gradient methods have a local view in the design variables space. The functional gradient on the point, defines the direction to get closer to optimum point. Depending on the starting point, after a few iterations, most of design variable space zones will lose their opportunity to contain the optimum point. Although these methods are fast, the final result dependent on the starting point commonly occurs whenever they are used for a nonlinear system, like a Stirling engine. It usually expressed as sticking to local optimums. Evolutionary algorithms such as genetic algorithm which use natural selection, mutation or recombination techniques to find the optimal point, reduce significantly the lack of sticking to local optimums but, in the other hand, they need numerous calls of calculation of engine performance which requires fast computer machines with significant time.

Neural networks can be used for optimization purposes [9]. In Refs. [10,11], neural network is applied to the end of predicting the power and performance of Stirling engines. For the purposes of this paper, this technique is used in order to define design parameters for optimizing the power and efficiency of Stirling engine. In fact, neural networks learn nonlinear and multivariable relations using large and rich set of data. Its main advantage consists in fast estimation of the output regarding to analytical algorithms and simulation codes. However, it should be trained for a new engine to have a suitable estimation of the output.

In this article, a new optimization procedure based on neural network concepts is presented. It has been used for ST500[2] Stirling engine, designed and fabricated by IPCO. The network could predict the engine output power and efficiency in a fraction of a second with less than 2% error. Neural networks have high capability to approximate multivariable and nonlinear functions and it would be able to predict engine outputs and efficiency for other Stirling designs similar to ST500. It is obvious that new engine data should be learned by network, for each new engine.

This is the first Stirling engine optimization procedure by means of a global view in the design variables space without needing numerous calls of calculation of engine performance.

As the First step, the engine is modeled thermodynamically to calculate the engine output power and the efficiency at some sample points in design variable space. According to these samples, the neural network will learn the relations between engine performance and variation of design variables. At the end, the network predicts the engine performance for the whole design space with specified resolution and finds the optimal point. Global view of this method against local view of some of previously used methods reduces the possibility of sticking to local optimum points. Moreover, the thermodynamic analysis takes significant time to calculate the engine performance for each sample point with enough accuracy. Using this method a minimum distance between the sample points have been kept in the design variables space to prevent excess calls of the thermodynamic analysis for areas of the space. This feature makes this method rather fast.

Another characteristic of this method is fast estimation of a Stirling engine performance, which is a benefit of using the neural network. Once the network is trained, it could be used in order to estimate the engine performance for specified conditions in fraction of a second. This benefit comes in handy for control purposes of FPSE[3] type which would be our next research step. It would help if the controller knows about the amount of energy being produced at any time. In Section 2, design variables are selected according to this purpose.

To determine the thermodynamic behavior of Stirling engine working fluid, there are a number of Stirling cycle analysis techniques. The techniques are categorized from zero to fourth order analysis. A zero order analysis is an experimental relation between engine output power and some of design parameters.

In a first order analysis, engine output power is calculated assuming ideal isothermal expansion and compression. For sinusoidal volume variations a closed form solution is also available [12].

Second order analysis is an extension of first order in which some power losses due to limitation of heat transfer and gas pressure drop and finally subtracted from isothermal calculation. Recently, Cheng [13] proposed a second order analysis which is suitable for prediction of thermal efficiency of a beta-type Stirling engine.

A third order analysis is a one-dimensional fluid modeling of working gas inside the engine to calculate power generation, heat transfer losses and pressure drop effects simultaneously.

Future detailed models like 3D modeling of working gas are classified in fourth order Stirling engine analysis. Makhkamov and Djumanov have presented a full 3D calculation of a Stirling engine using their CFD model in Ref. [14].

In this paper, calculation of engine performance is done using *Nlog thermodynamic analysis code*[4] which is a third order analysis. The code results verified by experimental data and its error is less than 18% for the cycle work. Then using the foregoing code, a set of data is produced. Accordingly, the neural network trained to recognize relations between inputs and outputs of the dataset. In the next step, the whole design variable space will be searched using the network to find the best optimum point. The procedure is done for *ST500* Stirling engine, with specifications shown in Table 1.

Fig. 2 shows the *ST500* Stirling engine used for the experiment. Heater, regenerator, cooler and compression space can be seen in this figure.

[1] Low Temperature Difference.

[2] Gamma-type Stirling engine manufactured by *IP-CO* (*Irankhodro power train company*).

[3] Free Piston Stirling Engines, type of Stirling engines in which piston and displacer are not mechanically connected to each other and freely oscillate inside their chambers. In this type, an external magnetic field releases the power generated by the engine and through this way controls the piston oscillation amplitude and phase on a specific frequency.

[4] Stirling engine third order analysis code, provided by Stirling machine researcher *M. Hooshang*(mazdak_hooshang@live.com)

Table 1
ST500 engine characteristics and operating conditions.

Specifications	Values
Type	Gamma
Electrical output power	500 W
Total efficiency	8.5%
Standard charge pressure	8 bars
Working fluid	Helium
Working frequency	14 Hz
Fuel	Natural gas
Cooling substance	Water
Power piston stroke	75 mm
Power piston diameter	84 mm
Displacer stroke	75 mm
Displacer diameter	97 mm
Phase angle	90 °
Heater type	Tubular (6 mm dia.) × 20
Cooler type	Duct (13 mm^2 section area) × 144
Regenerator material	Steel matrix (0.96 porosity)
Heat absorption temperature	350–420 °C
Heat rejection temperature	30–50 °C

2. Design & optimization variables

The target of this optimization process is to find the best value for design variables to keep the optimization variables as high as possible. Some of the engine parameters are assumed to be design variables and some others to be optimization variables. Generally, the target would be maximizing two variables ($H = 2$), engine output power and efficiency. Thus they are defined as optimization variables. Depending on the defined target, three design variables ($J = 3$) are selected including displacer stroke (d), engine frequency (f) and phase angle (φ).

Changing the displacer stroke affects on displacer swept volume and compression ratio. Compression ratio is the main design parameter for a Stirling engine to be adapted with wall temperature of engine heat exchangers. This parameter is also easy to apply on the real gamma-type engine against displacer bore or power piston bore and stroke. Changing the swept volume will change maximum fluid flow rate and velocity which is related to pumping loss in the heat exchangers. There are different ways to control the flow velocity but the easiest and effective way would be changing the engine working frequency. Increasing or decreasing engine frequency may also changes optimum phase angle [1].

Although there are many other variables affecting on the engine performance, these three variables are enough for a typical optimization procedure to converge to an optimal point while other engine specifications remain constant.

Both of the optimization variables represent the engine performance but to make a compromise, a weighted combination of them is defined in Eq. (3) (Variables $\overline{\eta}$ and $\overline{p}$ are normalized values of efficiency and output power respectively).

$$\Gamma = W\begin{bmatrix}\overline{\eta}\\ \overline{p}\end{bmatrix} \tag{3}$$

Consequently the optimization variable vector will be reduced to a scalar form, which is dependent to the weight vector of W. The weight vector is chosen arbitrary considering the fact that sum of the vector elements must be equal to unit.

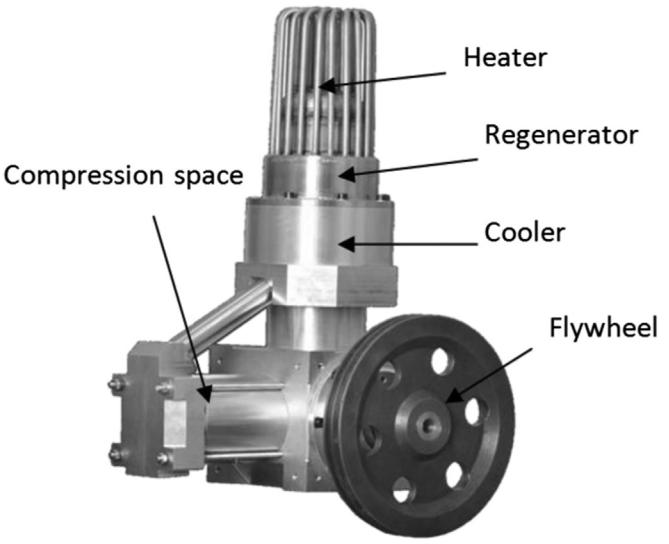

Fig. 2. Main parts of *ST500* Gamma type Stirling engine (Design and manufactured by IP-CO).

3. Design variable ranges and required precision

Required precision for determination of displacer stroke and phase angle is based on geometrical tolerances of engine manufacture. Required precision for determination of engine frequency also depends on dynamometer accuracy.

A reasonable range for all design variables are also determined from experience and are shown in Table 2.

4. Neural network

The total optimization procedure consists of two parts; pattern recognition and interpolation.

First, consider the engine model nature as a static transfer function. The engine model gets the design variables and gives output power and efficiency. While the inputs change, each of the outputs may uniformly ascend, uniformly descend or consecutively ascend and descend. There is also a situation in which some of input variations negate the others; thus the outputs may remain almost constant. For example, convective heat transfer coefficient in a heat exchanger pipe increases whenever the piston swept volume increases. But it may remain constant if engine working frequency decreases simultaneously.

Here is the role of the neural network to form such transfer function which can cover any of four discussed situations or even combination of them. Thus, a kind of pattern recognition procedure must be used which can support all these situations. Neural networks could act as a beneficial pattern recognition tool in which each neuron transfer function acts as a part of – discussed effects.

Above discussion lead us to a ridge-shape network transfer function. Structure of a sigmoid function, one of the well-known ridge-shape transfer functions, is shown in Eq. (4). In the forgoing equation, σ_i is weighted summation of input signals as formulated in Eq. (5) and y_i is output signal from neuron i (U_j is network input and w_{ji} is mid-layer weight).

Table 2
Design variable ranges and required precision.

Design variable	d: Displacer stroke (m)	ö: Phase angle (deg)	f: Frequency (Hz)
Minimum acceptable value	0.02	60	12
Maximum acceptable value	0.12	120	22
Required precision	±0.001	±0.25	±0.25

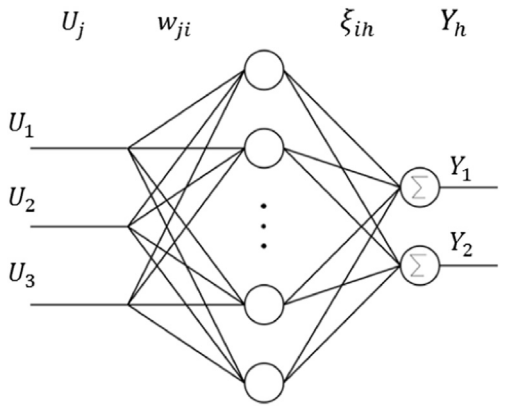

Fig. 3. MLP neural network model structure with one mid-layer, three inputs and two outputs.

$$y_i = (1 + \exp(-\sigma_i))^{-1} \tag{4}$$

$$\sigma_i = \sum_{j=1}^{J} w_{ji} U_j \tag{5}$$

In this paper, as presented in Fig. 3, a Multi-Layer Perceptron (MLP) neural network with one mid-layer and the sigmoid transfer functions for the mid-layer neurons is used. MLP is one of the best beneficial tools which is widely used for pattern recognition and classification [15].

According to Eq. (6), the network output is weighted summation of neuron output values. Therefore, while the network inputs increase (U_1,U_2 and U_3), depending on signs of ξ_{ih}s for each of neurons, the network outputs (Y_1 and Y_2) may increase, decrease, consecutively increase and decrease or remain constant. These are the four situations which the engine may respond.

$$Y_h = \sum_{i=1}^{I} \xi_{ih} y_i \tag{6}$$

A full input–output formula of this network can be formulated as follows:

$$Y_h = \sum_{i=1}^{I} \xi_{ih} \left(1 + \exp\left(-\sum_{j=1}^{J} w_{ji} U_j\right)\right)^{-1} \tag{7}$$

The network outputs are prediction of the network for engine output power and efficiency according to design variables discussed before.

5. Sample generation

In Section 2, three design variables are considered ($J = 3$) which makes the design variable a 3-dimensional space with 3 axes. The optimization objective is to determine these variables such that the maximum of output power and efficiency is obtained. On each axis, a number of grid points (z) are defined with equal distances. Combination of grid points creates total 3-dimensional sample points which are used to train the neural network. The total number of the sample points is equal to$q = z^J = z^3$. The engine power and efficiency at each sample point is calculated by the *Nlog code* (as explained in Section 8). Increasing the number of grid points on each axis, will raises the accuracy of network prediction along that direction but there is time limitation in calculation of power and efficiency. For each sample point, it takes at least 20 min using a machine with a T4500[5] CPU 4 GB of RAM.

According to trial and error, $z = 5$ seems to be adequate for all axes. ($z_1 = z_2 = z_3 = z$). Thus the network is trained via$q = 5^3 = 125$ samples. The total time spent for *Nlog code* to calculate power and efficiency of the sample points was about 50 h using the aforementioned machine.

The two inputs and three outputs of each sample are normalized according to the following expression to be fed into the network:

$$\overline{X} = \frac{X - \min(X)}{\max(X) - \min(X)}, X = p, \eta, d, \phi, f \tag{8}$$

6. Neural network training

A well-known method to train a MLP neural network is error back-propagation (BP) algorithm [16].

BP is an algorithm which decides to set the network weights (ξ and μ) such that the network output error is kept as low as possible. Network output error is defined considering engine output power and efficiency for each training sample as shown in what follows:

$$e_1 = \overline{p} - Y_1 \tag{9}$$

$$e_1 = \overline{\eta} - Y_2 \tag{10}$$

in which Y_1 and Y_2 are defined to be the network outputs.

Output power and efficiency of the engine are calculated using *Nlog code* for each value of design variables.

Network inputs are also normalized values of design variables where one has:

$$U_1 = \overline{d}, U_2 = \overline{\varphi}, U_3 = \overline{f} \tag{11}$$

At each step of training, network deviation factor is calculated according to BP algorithm using Eq. (12). Then required changes for the network weights are calculated using Eqs. (13) and (14). The learning rate in these two equations determines the speed of weights changes. Assuming a greater value makes the network weights to change more quickly (Quicker pattern learning) but may cause the weights to change unstably and prevent from a good convergence.

$$\delta_i = \frac{\partial y_i}{\partial \sigma_i} \sum_{h=1}^{H} e_h \xi_{ih} \tag{12}$$

$$\Delta\xi_{ih} = \gamma\, e_h\, y_i \tag{13}$$

$$\Delta w_{ji} = \gamma\, \delta_i\, U_j \tag{14}$$

New values for the network weights are set using following equations:

$$\xi_{ih}^{\text{new}} = \xi_{ih}^{\text{old}} + \Delta\xi_{ih} \tag{15}$$

$$w_{ji}^{\text{new}} = w_{ji}^{\text{old}} + \Delta w_{ji} \tag{16}$$

The training procedure is done with 5 epochs. At each epoch the total of $q = 125$ training samples are applied to the network so the total steps of network training is $5 \times 125 = 625$. As discussed

[5] A 2.3 GHz Dual-Core type CPU manufactured by Intel Inc.

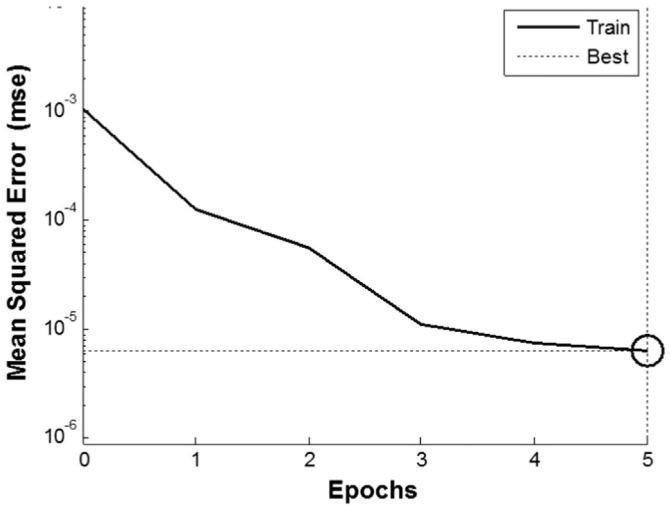

Fig. 4. Mean squared error against epochs during network training.

before, the network has three inputs ($j = 1,2,3$) and two outputs ($h = 1,2$).

Mean squared error during network training epochs is shown in Fig. 4 assuming 10 neurons for the network mid-layer and $\gamma = 0.7$ for the network learning rate.

In general, it is recommended to use simplest structure with minimum number of neurons to achieve fast interpolation with more reliability. Fig. 5 shows the variation of error norm for each network outputs according to the number of network mid-layer neurons. Thus 8 neurons for this layer makes the average error minimum and it is suitable for a better interpolation.

7. Determination of optimal point

To cover the full range of design variables space with precision specified in Table 2, estimation of engine output power and efficiency for 1.2×10^5 points is needed ($0.12 - 0.02/2 \times 0.001 \times 120 - 60/2 \times 0.25 \times 22 - 12/2 \times 0.25 = 1.2 \times 10^5$). Therefore the total 1.2×10^5 points dataset is fed to the network and the network predicts corresponding outputs for each one. Engine performance (Γ) which is weighted combination of the network outputs is calculated for each point using weight vector of $W = [0.7\ 0.3]$. These weight values are assigned due to importance

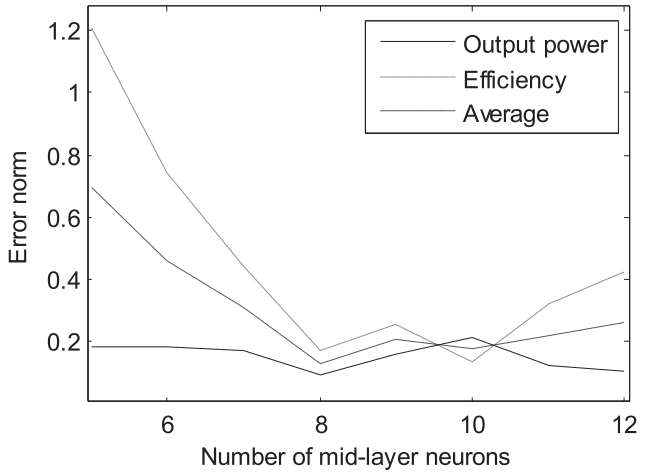

Fig. 5. Error norm according to number of mid-layer neurons.

Table 3
Neural network estimation comparison with *Nlog code* results for the achieved the optimal point.

Optimization variables	η	p
Neural network estimation	13.21%	878.2w
Nlog code result	13.45%	880.6w
Neural network estimation error	1.78%	0.27%

of Stirling engine working efficiency against output power but any arbitrary vector with summation of elements equal to unit could be assigned instead. Next the global maximum of Γ is determined. Denormalization of the network outputs for the maximum point results estimated engine output power and efficiency for the optimal point which are shown in Table 3. Calculation of the engine output power and efficiency on optimal point using *Nlog code* is also shown in Table 3.

Achieved optimal point for *ST500* engine is.

$$d_{opt} = 10.2\ \text{cm},\ \varphi_{opt} = 92.7\ \text{deg},\ f_{opt} = 18.4\ \text{Hz}$$

with output power and efficiency of:

$$p_{opt} = 880.6\ \text{W},\ \eta_{opt} = 13.45\%$$

while according to Table 1, previous operating point of the engine was:

$$d_{std} = 7.5\ \text{cm},\ \varphi_{std} = 90.0\ \text{deg},\ f_{std} = 14.0\ \text{Hz}$$

with output power and efficiency of:

$$p_{std} = 500\ \text{W},\ \eta_{std} = 8.50\%$$

Figs. 6–8 illustrate the variation of engine performance against two of three design variables while the third variable set to corresponding optimal point value.

Increasing 380 W of output power and 4.95% of efficiency shows the effectiveness of the optimization approach and low estimation error of neural network shows the considerable ability of MLP neural network to predict Stirling engine performance.

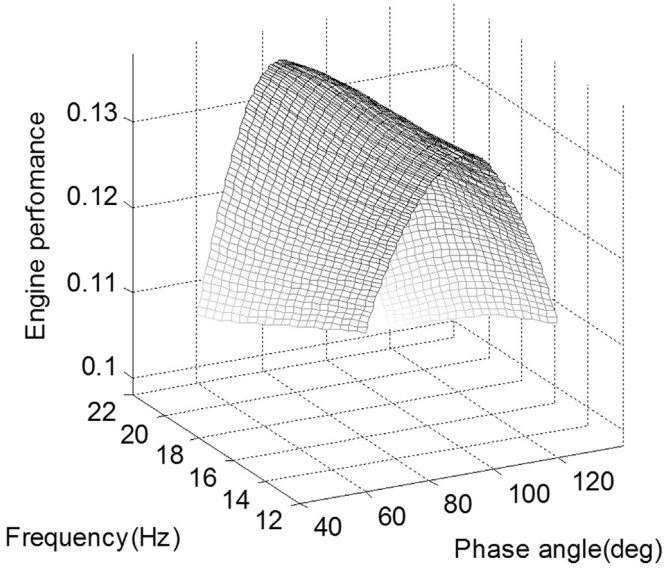

Fig. 6. Neural network output for engine performance against engine frequency and phase angle ($d = 10.2$ cm).

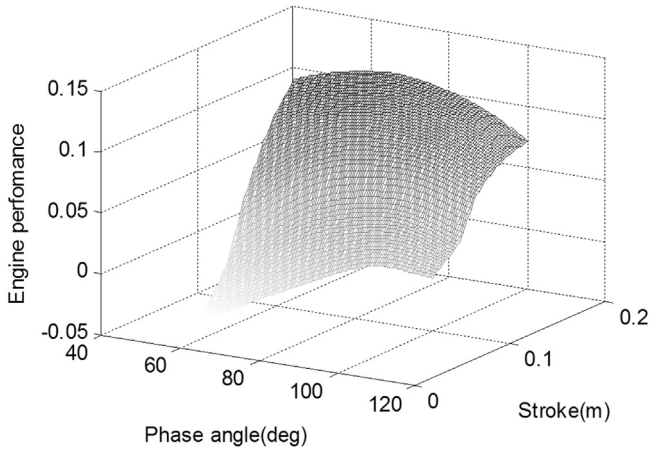

Fig. 7. Neural network output for engine performance against variation of stroke and phase angle ($f = 18.4$ Hz).

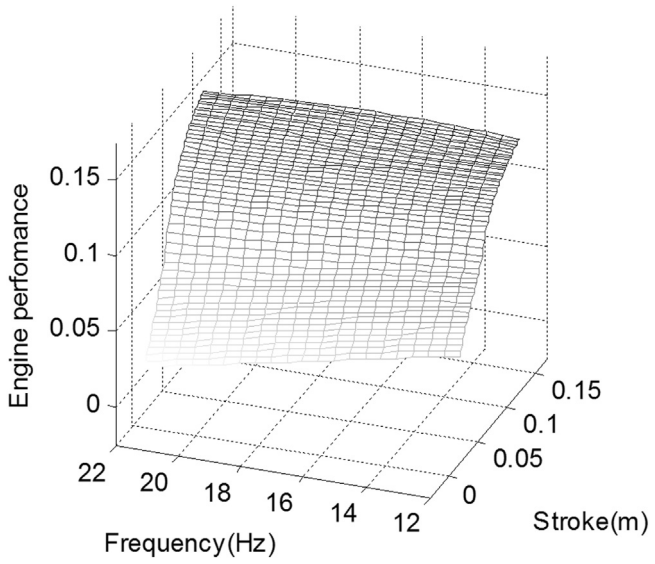

Fig. 8. Neural network output for engine performance against variation of frequency and stroke ($\varphi = 92.7$ deg).

8. *Nlog code* description

In this work, learning patterns are generated via *Nlog thermodynamic analysis code*. *Nlog* is a third-order Stirling cycle analyzer which calculates the generated power and rejected heat by Stirling engine and also instant working gas state variables according to following parameters of the engine:

1) Geometry properties of all gas transferring channels, pipes, and compression and expansion chambers.
2) Geometries of linkages between engine moving parts.
3) Engine initial charge pressure and local temperatures.
4) Temperature of heat exchangers wall (Constant during time period).

The code divides the whole gas transferring channels and pipes of the engine, to control volumes and determines gas dynamic and thermodynamic parameters for each control volume by solving continuity, momentum and energy equations simultaneously. Equations (17)–(19) are standard forms of continuity, momentum and energy equations respectively [17]. But they are simplified to the one-dimensional form which are fit for this third-order analysis.

$$\oint_{S_k} \rho v_f n \mathrm{d}A_f + \frac{\partial}{\partial t}\left(\int_{V_k} \rho \mathrm{d}V\right) = 0 \tag{17}$$

$$\frac{\partial}{\partial t}\left(\int_{V_k} \rho v_f \mathrm{d}V\right) + \int_{S_k} P n \mathrm{d}A_f + \int_{S_k} \left(v_f \rho\right) v_f n \mathrm{d}A_f + \tau_{f_k} A_{w_k} = 0 \tag{18}$$

$$\frac{\partial}{\partial t}\left(\int_{V_k} \left(\rho u + \rho \frac{v_f^2}{2}\right)\mathrm{d}V\right) + \int_{S_k} \left(\rho u + \rho \frac{v_f^2}{2} + P\right) v_f n \mathrm{d}A_f + \int_{S_k} P \frac{\mathrm{d}x}{\mathrm{d}t} n \mathrm{d}A_r - \frac{\mathrm{d}Q_c}{\mathrm{d}t} = 0 \tag{19}$$

Free flow area for the working gas transformation is assumed to be constant for each control volume thus Eq. (17) is converted to Eq. (20). The area is also assumed to be constant during time which leads to obtain Eq. (21).

$$\oint_{S_k} \rho v_f n \mathrm{d}A_f + \frac{\partial}{\partial t}\left(\rho_k A_{f_k} x_k\right) = 0 \tag{20}$$

$$\oint_{S_k} \rho v_f n \mathrm{d}A_f + A_{f_k} \frac{\partial}{\partial t}\left(\rho_k x_k\right) = 0 \tag{21}$$

Density and velocity of the working gas are assumed to be uniform over cross sectional area between adjacent control volumes and also inside each control volume. Thus following equation becomes the final simplified continuity equation used in the code.

$$\sum_{s=S_k} \rho_s v_{f_s} n_s A_{f_s} + A_{f_k} \frac{\partial}{\partial t}\left(\rho_k x_k\right) = 0 \tag{22}$$

Extending above assumptions of working gas velocity, density and cross sectional area, for working gas pressure in Eq. (18) will result in Eq. (23). The following is the simplified form of the momentum equation.

$$\frac{\partial}{\partial t}\left(\rho_k A_{f_k} x_k v_{f_k}\right) + \sum_{s=S_k} P_s n_s A_{f_s} + \sum_{s=S_k} \left(v_{f_s} \rho_s\right) v_{f_s} n_s A_{f_s} + \tau_{f_k} A_{w_k} = 0 \tag{23}$$

Energy equation is also simplified upon assuming gas specific heat to be equal for everywhere of each control volume and expressed as follows:

$$\frac{\partial}{\partial t}\left(\rho_k A_{f_k} x_k \left(u_k + \frac{v_{f_k}^2}{2}\right)\right) + \sum_{s=S_k} \left(\rho_s u_s + \rho_s \frac{v_{f_s}^2}{2} + P_s\right) v_{f_s} n_s A_{f_s} + A_{f_k} P_k \frac{\mathrm{d}x_k}{\mathrm{d}t} - \frac{\mathrm{d}Q_{c_k}}{\mathrm{d}t} = 0 \tag{24}$$

The total heat transferred into each control volume can be calculated using the following relation:

$$\frac{\mathrm{d}Q_{c_k}}{\mathrm{d}t} = \frac{Nu_k K_k A_{w_k}}{D_{h_k}} \left(T_{w_k} - T_k\right) \tag{25}$$

Variation of wall temperature for each control volume is calculated from:

$$\frac{dT_{w_k}}{dt} + \frac{1}{c_w m_{w_k}}\left(\frac{dQ_{c_k}}{dt} - \frac{dQ_{e_k}}{dt}\right) = 0 \tag{26}$$

Gas specific internal energy is assumed to be only function of gas temperature according to Eq. (27) for Helium gas [18]:

$$u_k = c_v T_k, \quad (c_v = 3.11\ \text{kJ/kg.K}) \tag{27}$$

Gas thermal conductivity is assumed to be function of gas temperature and pressure according to Eq. (28) for Helium gas [18].

$$K_k = 2.6810^{-3} \times \left(1 + 1.123 P_k 10^{-8}\right)\left(T_k^{.71\left(1-2\times10^{-9}P_k\right)}\right) \tag{28}$$

Thermodynamic Ideal gas behavior is considered and stated in Eq. (29) [18].

$$P_k = \rho_k r T_k, (r = 2.08\text{kJ/kg.K}) \tag{29}$$

Two assumptions are used by *Nlog code* depending on wall-type of each Stirling engine chambers. The assumption for a regenerative type walls is shown in Eq. (30-a) and for isothermal type is shown in Eq. (30-b).

$$\frac{dQ_{e_k}}{dt} = 0 \tag{30-a}$$

$$\frac{dT_{w_k}}{dt} = 0 \tag{30-b}$$

Formulations of Reynolds number (Re) and kinetic Reynolds number (Re_w) are described in Eq. (31) to Eq. (34).

$$Re_k = \frac{\rho_k v_{f_k} D_{h_k}}{\mu_k} \tag{31}$$

$$Re_{w_k} = \frac{\rho_k D_{h_k}^2 \dot{\theta}}{\mu_k} \tag{32}$$

$$\mu_k = 1.475 \times 10^{-6} \frac{T_k^{1.5}}{T_k + 80} \tag{33}$$

$$D_{h_k} = \frac{4 A_{f_k}}{A_{w_k}} \tag{34}$$

Fig. 9 represents the Kinematic modeling of the engine linkage. Referring to Fig. 9, φ, r_c, l_1, l_2, d, c_1, c_2 and a_1 to a_3 are engine construction parameters, i.e., design parameters, and are constant. Following equations relate these parameters to b_1 and b_2.

$$l_1^2 = r_c^2 + b_1^2 + 2 r_c b_1 \cos(\theta) \tag{35}$$

$$l_2^2 = r_c^2 + b_2^2 + 2 r_c b_2 \cos(\theta + \varphi) \tag{36}$$

Upon solving above equations for b_1 and b_2, they are expressed as functions of crank angle in Eq. (37) and Eq. (38). Thus x_1 to x_3 could be expressed as functions of crank angle according to Eqs. (39) and (41).

$$b_1 = \left(r_c^2 \cos^2\theta + l_1^2 - r_c^2\right)^{\frac{1}{2}} - r_c \cos\theta \tag{37}$$

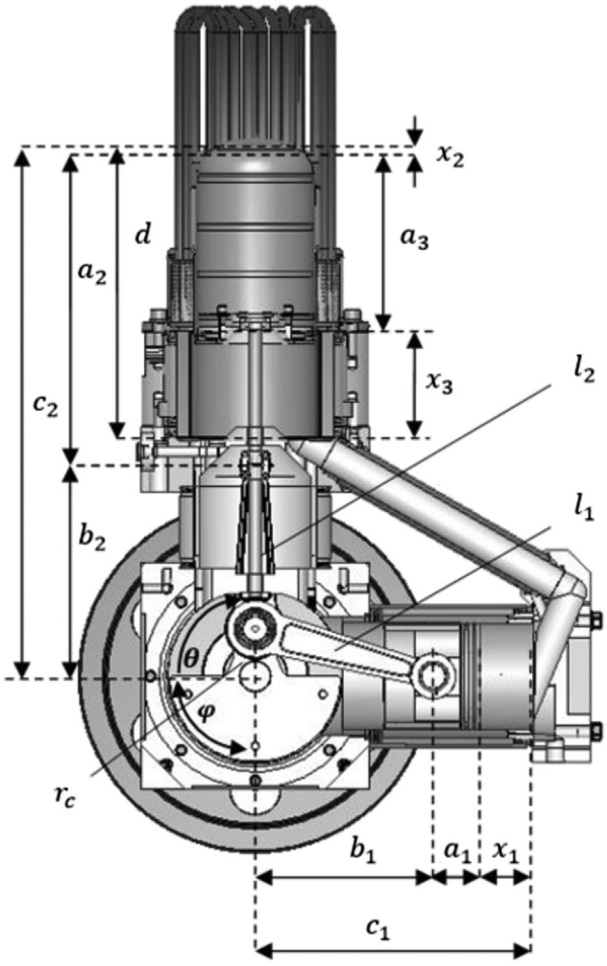

Fig. 9. ST500 linkage kinematics.

$$b_2 = \left(\frac{r_c^2 \cos(2\varphi + 2\theta)}{2} + l_2^2 - \frac{r_c^2}{2}\right)^{\frac{1}{2}} + r_c \cos(\varphi + \theta) \tag{38}$$

$$x_1 = c_1 - a_1 - b_1 \tag{39}$$

$$x_2 = c_2 - a_2 - b_2 \tag{40}$$

$$x_3 = d - a_3 - x_2 \tag{41}$$

For each control volume indexed by k, Eqs. (22)–(29) contain 12 unknown variables including x, τ, Nu, v_f, ρ, P, u, Q_e, Q_c, K, T_w and T. Depending on control volume index, the variable x is calculated from Eqs. 39 and 40 or (41) for variable volume chambers or set to constant for constant volume chambers. The values of τ and Nu are expressed as functions of Reynolds number (Re) and kinetic Reynolds number (Re_w) according to experimental correlations have been presented by Kays and London [19], De Monte et al. [20] [21] and S. Y. Zheng [22] for different ranges of Re and Re_w, type and dimensions of cross sectional area and wetted surface roughness for the engine heat exchangers.

Eqs. (22) and (30) totally form a system of 9 equations which *Nlog code* solves to determine 9 remained unknown variables at each time step for each control volume. The whole engine is divided

Table 4
Engine chambers and model control volumes.

Engine chambers	Control volumes
Piston	1 (k:1)
Connecting pipe	6 (k: 2–7)
Under displacer	1 (k: 8)
Cooler	7 (k: 9–15)
Regenerators (×5)	6 (k: 16–45)
Heater	7 (k: 46–52)
Above displacer	1 (k: 53)
Buffer	1 (k: 54)

to 11 chambers and 54 control volumes as shown in Table 4. A typical form of two adjacent control volumes is shown in Fig. 10. Runge Kutta 4th order method is used to solve the equations.

Finally, the results including engine output power, p, and rejected heat, $\dot{Q}_r$ are calculated as follows:

$$p = \sum_{\substack{\text{k:Variable}\\ \text{volumes}}} A_{f_k} P_k \frac{dx_k}{dt} \tag{42}$$

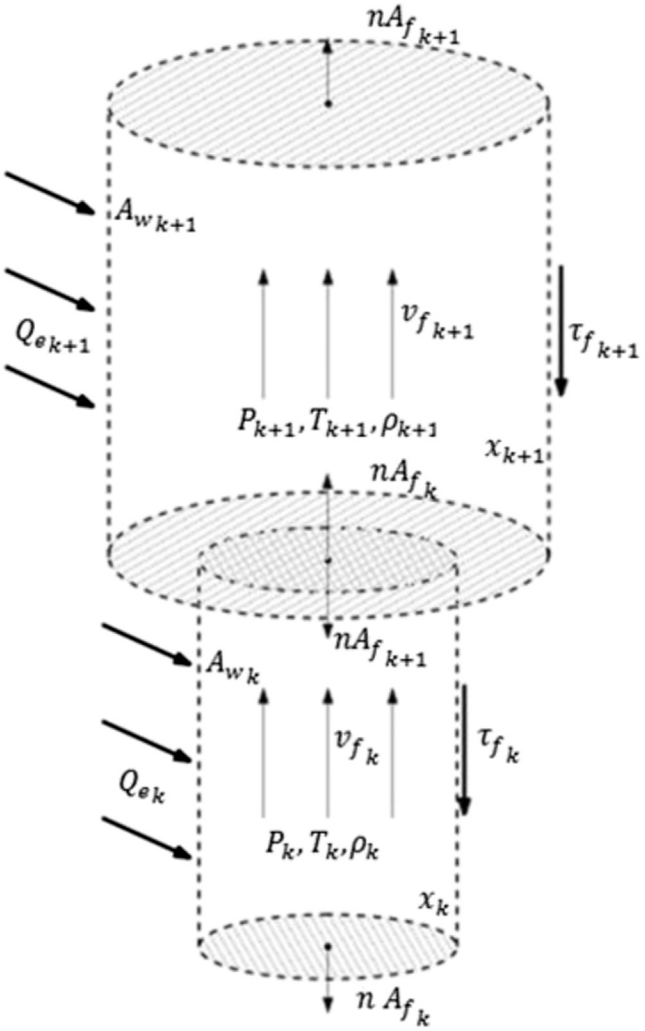

Fig. 10. Thermodynamic variables of two adjacent control volumes.

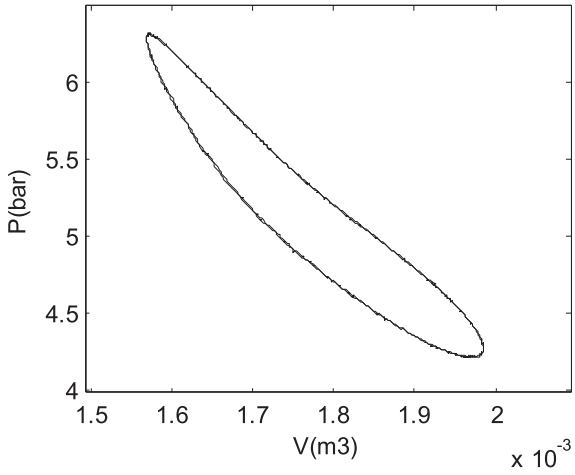

Fig. 11. Test results for condition C.

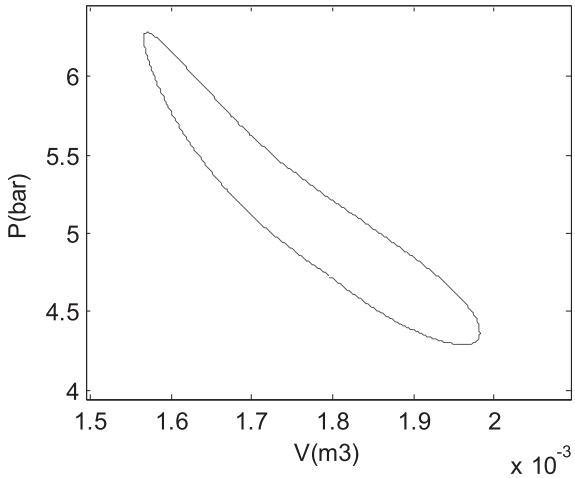

Fig. 12. *Nlog code* result for condition C.

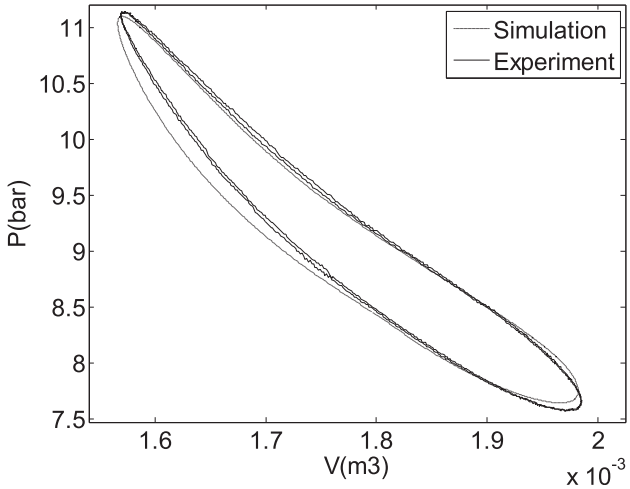

Fig. 13. Graphical comparison between test and *Nlog code* P–V diagrams for condition 'A'.

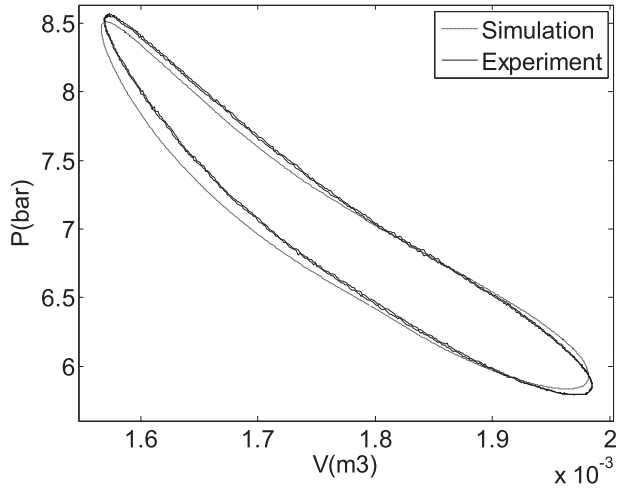

Fig. 14. Graphical comparison between test and *Nlog code* P–V diagrams for condition 'B'.

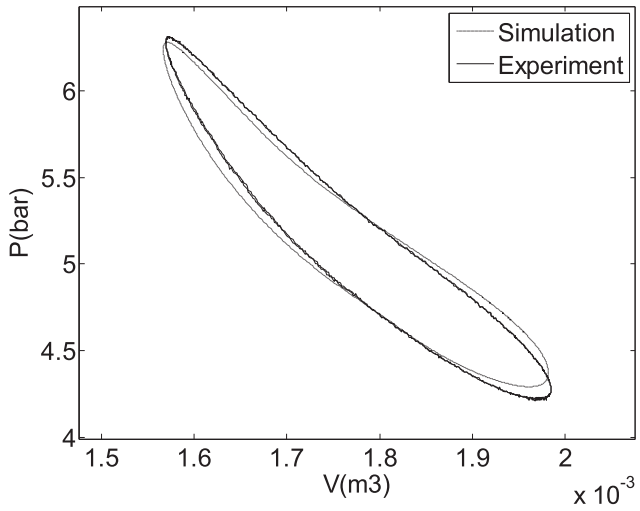

Fig. 15. Graphical comparison between test and *Nlog code* P–V diagrams for condition 'C'.

$$\dot{Q}_r = \sum_{\substack{\text{k:Cooler}\\ \text{volumes}}} \dot{Q}_{e_k} \tag{43}$$

The engine efficiency is calculated by Eq. (2) for the network training.

9. Thermodynamic analysis results validation

We need to make sure the *Nlog code* results to be reliable for this scope of study for optimization of *ST500* engine. Thus a test setup is established for the engine that measures critical state variables for some random situations to validate the code results.

For the validation, comparison for all the state variables of the test results and the code results along one time period could be done. But there are limitations for measuring some of the state variables like instant temperature of working gas which needs very low response-time sensors or piston position sensor which needs significant resistance against high temperatures for the sensor.

Thus the piston chamber gas pressure and engine crank angle were assumed to be instant test results because it is possible to measure them and rather easy to read by general data acquisition units. Other instant variables like the temperature and chamber volumes could be expressed as functions of gas pressure and crank angle according to state equation of ideal working gas (Eq. (29)) and geometries of engine linkages (Eqs. (35) & (36)).

A piezo-type pressure sensor[6] is placed at the top of the engine compression chamber. These types of sensors are vulnerable to high temperature and this is where the gas temperature is less than any other chambers. A cooling adapter[7] coupled to a water cooling system is also used to keep the sensor body temperature in acceptable range.

A crank angle encoder[8] is coupled to the engine flywheel. The encoder is a relative type but with trigger teeth it is used as an absolute type. According to tooth number, the crank angle and total working volume of the engine is calculated.

Average value of the engine rejected heat also could be calculated simply by measuring coolant liquid flow, coolant entrance temperature and coolant exit temperature.

The whole test setup for *ST500* engine is shown in Fig. 16.

All of boundary conditions during the test were kept near to engine standard specifications presented in Table 1.

The test is done on *ST500* engine for three different charge pressures (Represented as initial conditions) and heat exchanger wall temperatures (Represented as boundary conditions) which are shown in Table 5.

P–V diagram for condition 'C' is shown in Fig. 11 which is a graphical result of the test.

All of the *ST500* engine specifications (Table 1) are put into the *Nlog* code. Initial conditions of working gas pressure and boundary conditions of heat exchanger wall temperatures are set same as the test rig condition (Table 5).

The code is run on a machine explained before. Total spent time for the machine was about 70 min 50 min to simulate engine warm up period (Equivalent to three complete cycles), and about 20 min to obtain main results (Equivalent to one complete cycle). P–V diagram for condition 'C' is shown in Fig. 12 which is a graphical result of the code.

Comparisons between the test and code results for three different conditions (Table 5) are shown in Table 6. As shown in this table, the maximum estimation error is about 11% for power and about 18% for rejected heat rate. All power losses of dynamometer system (Including the belt, magnetic field and electric losses of generator wiring) are pre-calculated and compensated by data accusation software. The code doesn't take into account mechanical losses due to bearings and rings. In order to have a rough estimation of these losses, friction loss value[9] of the engine is extended for higher frequencies and added to experiments results values. It should be noted that due to the non-oil lubrication of the engine, it is possible to consider linear behavior for bearing friction factor.

This prediction error level is low enough for an optimization procedure comparing with some other Stirling cycle analysis codes. For example, the errors of same comparison between uncalibrated[10] version of *GLIMPS*[11] code calculations and experimental

[6] Instant pressure sensor of *Kistler* 4075A.
[7] Compact cooling adapter of *Kistler* 7505B.
[8] Crank angle encoder of 365-series.
[9] Test which is performed by the engine manufacturer to determine internal dry friction losses of it at low frequencies.
[10] Only results of uncalibrated version of the codes is valuable for a design or optimization procedure.
[11] Stirling cycle analysis code being used by National Aeronautics and Space Administration (NASA).

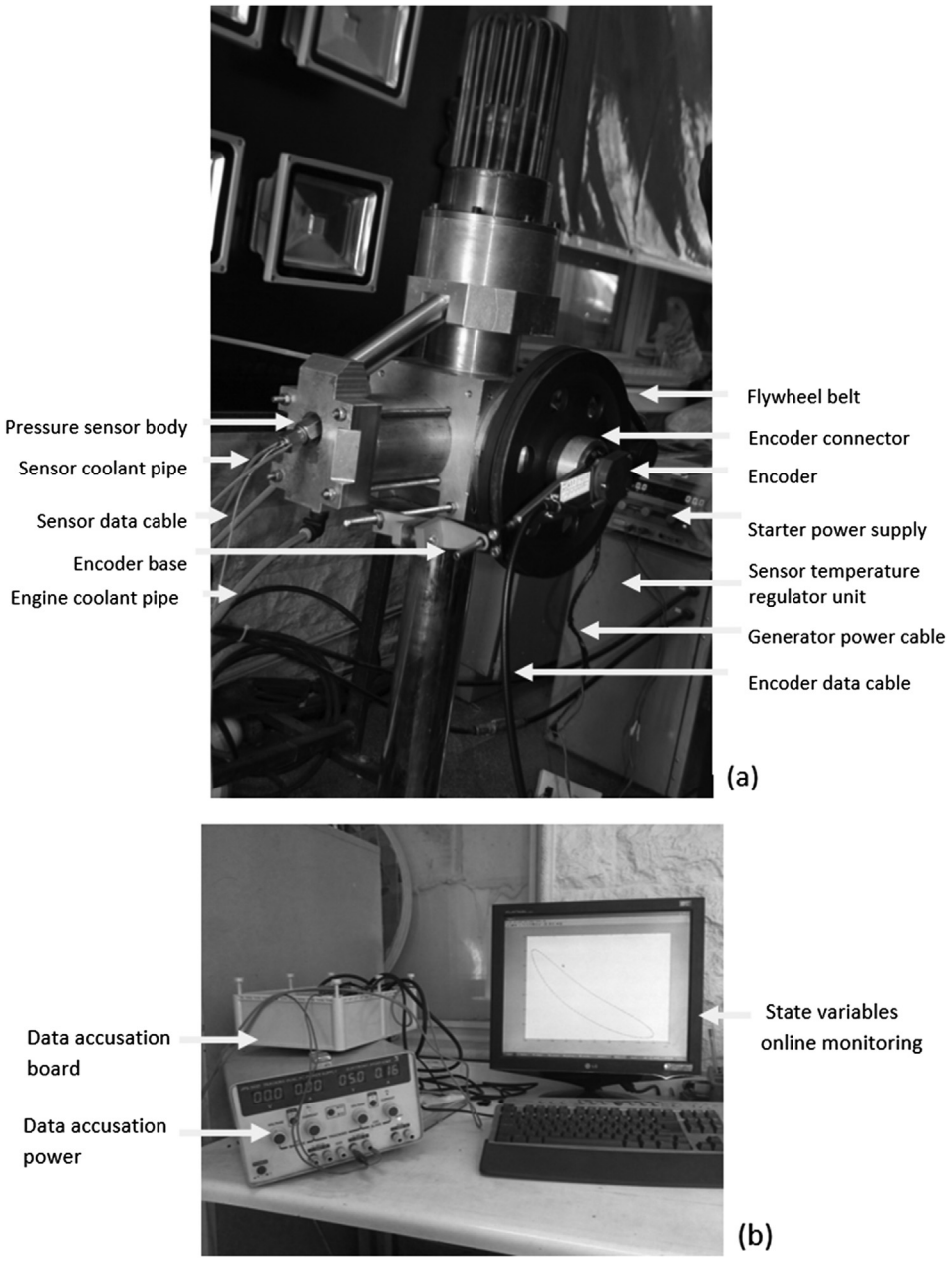

Fig. 16. (a) *ST500* engine test setup, (b) Data accusation unit.

measurements of *RE-1000*[12] engine are 1.5% for rejected heat and 19.0% for power [23].

Comparisons between overall curve shapes of P–V diagrams for three different conditions (Table 5) are shown in Figs. 13 to 15.

There is also an adequate compliance for overall curve shapes of P–V diagrams. Area inside the P–V diagrams represents the power exchanging between engine pistons and working gas.

10. Conclusion

In this article, an optimization procedure for Stirling engines using neural network was presented. Choosing MLP neural network for this kind of pattern recognition problem was because of the ridge-shape transfer functions nature which enables the network to predict engine performance fast enough and precise. It was shown that via 8 mid-layer neurons, the network could predict the engine output power and efficiency in a fraction of a second with

Table 5
Three different initial and boundary conditions.

Condition	A	B	C
Charge pressure (bar)	8.1	6.2	4.6
Coolant liquid flow (lit/min)	6.1	6.1	6.1
Coolant entrance temp. (′C)	33.5	40	35
Coolant exit temp. (′C)	41.0	46	42
Heater tip temp. (′C)	393	400	395
Heater base temp. (′C)	353	350	355

[12] A 1 kW free piston Stirling engine designed by Sunpower Inc.

Table 6
Comparison between *Nlog code* and experimental measurements of *ST500* engine.

Condition		A	B	C
Nlog Code	Rejected heat rate (kW)	3.331	2.974	2.270
	Power (kW)	0.440	0.363	0.262
Experiment	Rejected heat rate (kW)	2.94	2.52	2.52
	Power (kW)	0.400	0.343	0.235
Error	Rejected heat rate (%)	13.2	17.8	9.9
	Power (%)	10.0	5.8	11.4

less than 2% error (compared to the thermodynamic code result) while the thermodynamic code takes at least 20 min for one simulation session. Defining more design variables obviously takes into account more relations between inputs and outputs, so the number of the neurons must be increased to keep estimation error at low levels. Spacing of training samples along each input axes, also affect on network prediction quality; but according to trial and error it is determined that 5 points for each axis is enough to cover the whole common ranges of many design variables.

Comparison between engine output power and rejected heat for test setup and *Nlog thermodynamic analysis code* in same conditions, represented acceptable compliance, so the code results could be accepted. Confirmation of 878 W of output power and 13.21% of efficiency by the code comparing 500 W and 8.5% for the engine before the optimization, illustrates the advantageous of optimization procedure using the neural network.

Acknowledgment

The experiment phase of this work is done in *Stirling engine laboratory* of Irankhodro power train Company, *IP-CO*. Particular appreciation is expressed to *IP-CO* staff, Mr. Alizadeh, Damirchi and Ehteram for their aids and supports.

References

[1] Martini WR. Stirling engine design manual. National Aeronautics and Space Administration (NASA); 1983. CR-168088.
[2] Thimsen D. Stirling engine assessment. 2002.
[3] Yaqia L, Yalinga H, Weiweia W. Optimization of solar-powered Stirling heat engine with finite-time thermodynamics. Renew Energy 2011;36:421–7.
[4] Toropov VV. Multipoint approximation method in optimization problems with expensive function values. Computational system analysis. 1992. p. 207–12.
[5] Hirata K. Mechanical loss reduction of a 100 W Class Stirling engine. In: 11th International Stirling Engine Conference; 2003. p. 338–43.
[6] Timoumi Y, Tlili I, Nasrallah SB. Performance optimization of Stirling engines. Renew energy 2008:2134–44.
[7] Kraitong K, Mahkamov K. Optimization of low temperature difference solar Stirling engines using genetic algorithm. In: World Renewable Energy Congress, Sweden; 2011. p. 3945–52.
[8] Chen C-L, Ho C-E, Yau H-T. Performance analysis and optimization of a solar powered Stirling engine with heat transfer considerations. Energies 2012: 3573–85.
[9] Zhang XS. Neural networks in optimization. Springer; 2000.
[10] Ahmadi MH, Aghaj SSG, Nazeri A. Prediction of power in solar stirling heat engine by using neural network based on hybrid genetic algorithm and particle swarm optimization. Neural Comput Appl 2012:1141–50. Springer.
[11] Kiani MKD, Ghobadian B, Tavakoli T, Nikbakht AM, Najafi G. Application of artificial neural networks for the prediction of performance and exhaust emissions in SI engine using ethanol- gasoline blends. Energy Convers Manag 2010:65–9.
[12] Dyson RW, Wilson SD, Tew RC. Review of computational Stirling analysis methods. National Aeronautics and Space Administration (NASA); 2004.
[13] Cheng C-H, Yu Y-J. Numerical model for predicting thermodynamic cycle and thermal efficiency of a beta-type Stirling engine with rhombic-drive mechanism. Renew Energy 2010;35:2590–601.
[14] Makhkamov K, Djumanov D. Three-dimensional CFD modeling of a Stirling engine. In: Stirling Engine Conference, Rome, Italy; 2003.
[15] Hu YH, Hwang J-N. Handbook of neural network signal processing. CRC Press; 2001.
[16] Fausett LV. Fundamentals of neural networks: architectures, algorithms, and applications. J. N.. 1994
[17] Fox RW, McDonald AT, Pritchard PJ. Introduction to fluid mechanics. USA: John Wiley & Sons, Inc.; 2004.
[18] Petersen H. The properties of helium: density, specific heats, viscosity and thermal conductivity at pressures from 1 to 100bar and from room temperature to about 1800K. 1970.
[19] Kays WM, London AL. Compact heat exchangers. McGraw Hill; 1984.
[20] Monte Fd, Galli G, Marcotullio F. An analytical oscillating-flow thermal analysis of the heat exchangers and regenerator in Stirling machines. In: Energy Conversion Engineering Intersociety Conference; 1996. p. 1421–7.
[21] Monte Fd. Thermal analysis of the heat exchangers and regenerator in Stirling cycle machines. J Propuls Power 1997:404–11.
[22] Zheng SY. Oscillatory flow and heat transfer in Stirling engine regenerator. PhD thesis. Case western reserve university; 1993.
[23] Geng SM, Tew RC. Comparison of GLIMPS and HFAST Stirling engine code predictions with experimental data. 1992.